Published in final edited form as:

ACS Appl Mater Interfaces. 2017 July 12; 9(27): 22994–23006. doi:10.1021/acsami.7b06103.

Tunable Surface Repellency Maintains Stemness and Redox Capacity of Human Mesenchymal Stem Cells

Daniel A. Balikov[†,‡,$], **Spencer W. Crowder**[†,‡,%,$], **Timothy C. Boire**[†], **Jung Bok Lee**[†], **Mukesh K. Gupta**[†], **Aidan M. Fenix**[§], **Holley N. Lewis**[†], **Caitlyn M. Ambrose**[†], **Philip A. Short**[†], **Chang Soo Kim**[‖], **Dylan T. Burnette**[§], **Matthew A. Reilly**[⊥], **N. Sanjeeva Murthy**[#], **Mi-Lan Kang**[⊗], **Won Shik Kim**[∇], and **Hak-Joon Sung**[*,†,‡,⊗]

[†]Department of Biomedical Engineering, Vanderbilt University, Nashville, Tennessee 37235, United States

[‡]Center for Stem Cell Biology, Vanderbilt University Medical Center, Nashville, Tennessee 37232, United States

[§]Department of Cell and Developmental Biology, Vanderbilt University Medical Center, Nashville, Tennessee 37232, United States

[‖]Department of Materials Science and Engineering, University of Wisconsin, Milwaukee, Wisconsin 53211, United States

[⊥]Department of Biomedical Engineering, The Ohio State University, Columbus, Ohio 43210, United States

[#]Department of Biomedical Engineering, Rutgers University, Piscataway, New Jersey 08854, United States

[⊗]Severance Biomedical Science Institute, College of Medicine, Yonsei University, Seoul 120-752, Republic of Korea

[∇]Department of Otorhinolaryngology, College of Medicine, Yonsei University, Seoul 120-752, Republic of Korea

Abstract

Human bone marrow derived mesenchymal stem cells (hMSCs) hold great promise for regenerative medicine due to their multipotent differentiation capacity and immunomodulatory

---

[*] **Corresponding Author:** hak-joon.sung@vanderbilt.edu.

[%] **Present Address:** (S.W.C.) Department of Materials and Department of Bioengineering, Imperial College London, London, UK.

[$] **Author Contributions:** D.A.B. and S.W.C. contributed equally to this work.

Supporting Information

The Supporting Information is available free of charge on the ACS Publications website at DOI: 10.1021/acsami.7b06103.

Additional figures, primer sequences for qPCR, and antibody details (PDF)

ORCID

Matthew A. Reilly: 0000-0001-8029-0084

Won Shik Kim: 0000-0002-1264-5354

Hak-Joon Sung: 0000-0003-2312-2484

Notes

The authors declare no competing financial interest.

capabilities. Substantial research has elucidated mechanisms by which extracellular cues regulate hMSC fate decisions, but considerably less work has addressed how material properties can be leveraged to maintain undifferentiated stem cells. Here, we show that synthetic culture substrates designed to exhibit moderate cell-repellency promote high stemness and low oxidative stress—two indicators of naïve, healthy stem cells—in commercial and patient-derived hMSCs. Furthermore, the material-mediated effect on cell behavior can be tuned by altering the molar percentage (mol %) and/or chain length of poly(ethylene glycol) (PEG), the repellant block linked to hydrophobic poly(ε-caprolactone) (PCL) in the copolymer backbone. Nano- and angstrom-scale characterization of the cell-material interface reveals that PEG interrupts the adhesive PCL domains in a chain-length-dependent manner; this prevents hMSCs from forming mature focal adhesions and subsequently promotes cell–cell adhesions that require connexin-43. This study is the first to demonstrate that intrinsic properties of synthetic materials can be tuned to regulate the stemness and redox capacity of hMSCs and provides new insight for designing highly scalable, programmable culture platforms for clinical translation.

Graphical abstract

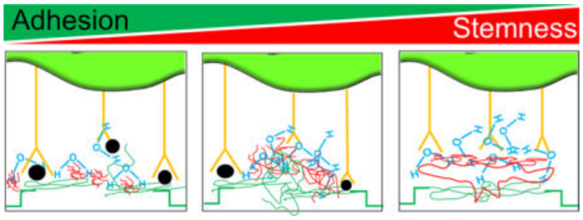

Keywords

polymers; biomaterials; stem cells; regenerative medicine; cell-matrix interface

INTRODUCTION

The application of human bone marrow derived mesenchymal stem cells (hMSCs) to tissue engineering and regenerative medicine has received immense attention over the past decade. Encouraging results from basic science studies have stimulated a worldwide interest in the use of hMSCs for treating human diseases, and hundreds of clinical trials are currently underway.[1,2] Despite the promise of hMSCs, aging patients who stand to benefit the most from these therapies have a declining number of resident stem cells, and those that remain exhibit crippling abnormalities, such as reduced proliferation rate and differentiation capacity, which severely limit their therapeutic efficacy.[3,4] Furthermore, hMSC-mediated tissue regeneration would require exhaustive in vitro expansion to achieve relevant numbers for stem cell therapies, and serially expanded hMSCs demonstrate passage-associated abnormalities that further limit their therapeutic potential.[5,6] In order to realize clinical translation, new strategies to maintain or reinstate hMSC fitness following expansion must be developed to counteract this inherent decline in cell health.[7]

Cell–matrix and cell–cell interactions are known to instruct stem cell behavior. Within their in vivo niche, stem cells are anchored to the extracellular matrix and neighboring cells, and the competition between these interactions is instrumental for maintaining stemness or inducing differentiation. Several groups within the biomaterials community are attempting to elucidate how hMSCs sense their environment as well as identify how the “sensing” is transduced to elicit functional change in cell phenotype.[8–11] However, most biomaterial systems encourage cell–matrix adhesion, yet biasing the cells in the opposite direction (i.e., toward cell–cell interactions) can be equally beneficial to understand hMSC biology and utilize this new knowledge to therapeutic applications. For example, hMSCs cultured as substrate-free aggregates, or “hanging drops” (HDs), are initially comprised of only cell–cell contacts and have garnered attention due to their anti-inflammatory capabilities.[12] These methods have relied upon forced aggregation or repellant surfaces to cluster the hMSCs, which raises two important points: (1) cell–substratum interactions, an inarguably critical component of stem cell homeostatic mechanisms, are absent in these systems, focusing instead only on cell–cell interactions and the extracellular matrix (ECM) molecules produced locally within the aggregates, and (2) although hMSC spheroids exhibit improved therapeutic potential as producers of pro-angiogenic/anti-inflammatory signals,[13] their use for in vivo implantation is severely limited because HDs pose technical problems for clinical translation, including scalability, handling, and implantation.

In contrast to HD assemblies, material systems such as patterned surfaces,[14] prefabricated microwells,[15] or chitosan-based substrates[16,17] can be leveraged to promote cell aggregation, but in-depth analysis of the structure–function relationship between the material composition/properties and subsequent cellular response remains undeveloped. Nevertheless, numerous studies have investigated the mechanisms by which hMSCs aggregate, as well as the resulting changes to their therapeutic profile, but these have typically relied upon nonadhesive plates or suspension cultures instead of providing a material to which the cells can bind and upon which can form a dynamic, natural aggregate.[18] To address this issue, synthetic copolymer culture substrates can simultaneously provide physicochemical cues that encourage HD-like cell behaviors while simultaneously allowing tuning of the material composition, and subsequent properties, for in-depth analysis of material-mediated regulation of the cellular response.

In this study, we designed copolymers of varying surface repellency that effectively modulate both stemness and redox regulation in hMSCs, and demonstrate that these effects can be finely tuned by altering the polymer composition. We further show that nanoscale interactions between the copolymer subunits have a functional consequence on how cells perceive and adhere to the material surface, which subsequently changes their transcriptional program. Of particular importance, the cell-instructive effects observed on the copolymer substrates directly result from the entropic organization of the competing poly(ethylene glycol) (PEG) and poly(ε-caprolactone) (PCL) chains, representing a cheap and scalable platform for modulating cell behavior in a clinical setting without the need for pre- or postprocessing. These data represent substantial progress in understanding how intrinsic properties of polymeric culture substrates–that is, without preprogramming physicochemical cues into the material substrate–give rise to changes in the functionality of human stem cells, and provide insight for developing new culture materials for therapeutic applications.

MATERIALS AND METHODS

Polymer Substrate Preparation

All polymers were synthesized as previously described.[19] Unless otherwise noted, all *in vitro* experiments were performed on spin-coated polymer films that were prepared with a commercial spin-coater (Laurell Technologies, North Wales, PA). Fifteen millimeter circular glass coverslips (Fisher Scientific, Waltham, MA) or 10 cm Pyrex Petri dishes (Corning, Inc., Corning, NY) were first cleaned with 100% ethanol (Sigma-Aldrich, St. Louis, MO), rinsed with dH_2O, and heated to 80 °C for ~20 min to dry. A 1% weight/volume (w/v) solution of the specified polymer in tetrahydrofuran (THF, Sigma-Aldrich) was spun for either 30 s at 3000 rpm on glass coverslips (50 μL solution/sample) or 2 min at 1500 rpm on Petri dishes (1 mL solution/sample). All samples were then exposed to a constant cold-trap vacuum for ≥30 min to remove excess solvent and kept in a desiccator until use. For cell experiments, substrates were UV sterilized for 30–60 min on each side before use; for 15 mm cover glass, samples were placed in a 24-well plate and secured with an autoclaved silicon O-ring (McMaster Carr, Atlanta, GA).

For protein precoating experiments, the desired amount of human fibronectin (Fisher Scientific) was diluted in serum-free αMEM and allowed to adsorb to the material surface for ≥30 min at 37 °C. Samples were then rinsed twice with PBS and used for culture experiments.

Physicochemical Characterization of Polymer Surfaces

Protein adsorption was measured by quartz crystal microbalance with dissipation (QCM-D). Polymer was spin coated onto gold-coated quartz crystal (5 MHz, QSX 301; Q-Sense AB, Goetenberg, Sweden) using a ~50 μL of 10 mg/mL solution at 3000 rpm for 30 s using a spin coater (Headway Research Inc., TX). QCM-D measurements were carried out using a Q-Sense E4 instrument (Q-Sense AB, Goetenberg, Sweden) at 37.5 °C with 10% FBS, according to standard protocols.[20] The data were analyzed using the Voigt model in the Q Tools software supplied by Q-Sense, Inc. Contact angle was performed with a goniometer (Ramé-Hart, Succassunna, NJ) using 10 μL droplets of deionized water. Three measurements were taken on each of three independent samples, and the average advancing contact angle was reported ($n = 9$).

Elastic surface modulus near the surface, which is sometimes referred to as surface modulus or Young’s modulus, was measured using a Veeco NanoScope V (Bruker Corporation, Billerica, MA) using a cantilever with a rectangular cross-section (MLCT tip B; Bruker AFM Probes). A glass coverslip was used as a control sample, while all spin-coated coverslips were tested using an identical protocol. Samples were first incubated in PBS overnight before testing in air at 37 °C. A topographical scan of a 5 μm × 5 μm area was made in contact mode sampling 512 samples/line for 512 lines with a scanning rate of 30 μm/s. A z-limit of 5 μm was used to prevent tip failure. A force volume scan was then performed to allow for an estimation of the sample’s area-averaged elastic modulus. A 16 × 16 grid spanning the same area as the topographical scan was indented at 1.54 μm/s to a maximum motor movement of 750 nm. Calibration of the deflection-voltage curve $d(V)$ of the cantilever beam was estimated using a series of indentations into a glass coverslip by assuming rigidity of the coverslip. This calibration had the form

$$d\,(\mathrm{nm}) = 0.0000113V^2 + 0.00836V - 12.3$$

where V has units of volts ($n = 3$; $R^2 = 0.997$). The Sader method[21] was used to estimate the cantilever stiffness k (approximately 0.02 N/m) such that the force could be estimated as $F = kd$. The indentation depth u was computed as

$$u = (P - P_c) - (d - d_c)$$

where P is the absolute position of the stage, P_C is the absolute position at the point of contact between the tip and the sample, and d_C is the deflection of the cantilever at the point of contact. This allowed the generation of a force–displacement $F(u)$ diagram for each sample point in the force–volume image. These data were then analyzed using conical indenter theory corrected for the true probe geometry.[22] These results were then used to estimate the elastic modulus E in a least-squares sense by treating it as a parameter in a Levenberg–Marquadt fitting algorithm. The expected form of the $F(u)$ data was given by

$$F(u) = \frac{2\beta tan\alpha}{\pi}\frac{E}{1-\upsilon^2}u^2$$

where α is the half angle of the indentation probe (nominal average 71.25°) and $\beta = 1.023$ is the asymmetric correction factor for a probe with square base,[22] assuming incompressibility (i.e., Poisson ratio $\nu = 0.5$) and rigidity of the indentation probe. The area-averaged elastic modulus was then found by averaging the modulus determined for each of equally spaced 256 locations within the 5 μm × 5 μm area characterized during the topographical scan. Analysis was performed using NanoScope Analysis v1.50 (Bruker). Ten randomly selected locations were analyzed using the indentation analysis tools in this software package. Data from 10 to 70% of the full force scale were included in the analysis.

^{1}H NMR was conducted on a 400 MHz AV-400 console (Bruker Instruments, Inc.) using 1% w/v solutions in $CDCl_3$. The mole percent composition for each copolymer was determined by comparing the integration of CH_2CH_2 protons of PEG ($\delta = 3.65$ ppm) to that of OCH_2 protons representing the ε-carbon of the PCL peak at ($\delta = 4.05$ ppm).[23]

Molecular weight was measured by gel permeation chromatography. After dissolving copolymers in THF at 10% w/v, the polymer solutions were injected at 1 mL/min through a Waters chromatography system equipped with a binary HPLC pump, refractive index detector, dual λ absorbance detector, and four 5 mm Waters columns (300 mm × 7.7 mm) connected in series (Waters Corporation, Milford, MA).[24]

PEG volume percent was calculated using three equations. First, PCL molecular weight for each copolymer was calculated using

$$\mathrm{PCL}\ M_W = \mathrm{copolymer}\ M_W - \frac{(\mathrm{PEG\ mol\%} \times \mathrm{PEG}\ M_W)}{100}$$

PEG molecular weight was taken from the manufacturer's data sheet and copolymer molecular weight reported by gel permeation chromatography. Weight percent of PEG or PCL in each copolymer was then calculated using

$$\mathrm{PEG\ wt\%} = \frac{100\,(\mathrm{PEG\ mol\%} \times \mathrm{PEG}\ M_W)}{(\mathrm{PEG\ mol\%} \times \mathrm{PEG}\ M_W + \mathrm{PCL\ mol\%} \times \mathrm{PCL}\ M_W)}$$

Finally, PEG volume percent of each copolymer was calculated using

$$\mathrm{PEG\ vol\%} = \frac{100\left(\frac{\mathrm{PEG\ wt\%}}{1.234}\right)}{\left(\frac{\mathrm{PEG\ wt\%}}{1.234} + \frac{\mathrm{PCL\ wt\%}}{1.146}\right)}$$

where 1.234 and 1.146 are the densities (g/cm^3) of PEG and PCL, respectively.

For X-ray scattering experiments, Pyrex Petri dishes were spin-coated with 40% w/v copolymer solutions in THF. Each Petri dish was spun twice to generate a film that could be peeled off the dish surface by hand and easily handled for transportation and cut to size for insertion into 2 mm quartz capillary tubes. X-ray scattering was performed before (dry conditions) and after wetting by exposing polymers to phosphate buffered saline (PBS) for at least 6 h. Small- and medium-angle X-ray scattering was performed at the Cornell High Energy Synchrotron Source (CHESS) facility in Ithaca, NY. The wavelength was 1.055 Å, and sample-to-detector distances were 1479 and 416 mm for small- and medium-angle scattering, respectively. Radiation damage was monitored by collecting 10 exposures, each of 4 s duration, and no radiation damage was observed. Small- and medium-angle X-ray scattering data were analyzed using BioXTAS RAW 0.99.14b software (open-source on sourceforge.net). Wide-angle X-ray scattering data were collected on a Bruker area detector using Cu Kα radiation from a rotating anode and a sample-to-detector distance of 88 mm. These data were analyzed using JADE software (Materials Data Inc., Livermore, CA).

Cell Culture

hMSCs were either purchased from Lonza (Walkersville, MD) or acquired from patients aged over 65 years old at Vanderbilt University Medical Center in cooperation with Dr. Pampee P. Young, according to previously published methods (Figure S9 for surface marker phenotype data).[25] hMSCs were maintained in complete media (CM) composed of α-minimum essential media with nucleosides (αMEM, Life Technologies, Carlsbad, CA) with 16.7% fetal bovine serum (Life Technologies), 1% penicillin/streptomycin (Life Technologies), and 4 μg/mL plasmocin (InvivoGen, San Diego, CA). Cells were kept in a humidified incubator at 37 °C and 5% CO$_2$, and media was replaced twice each week. When ~80% confluent, hMSCs were detached with 0.05% trypsin-EDTA, reseeded at a density of 100–500 cell/cm^2, and cultured for 7–14 days before reaching confluence. For all experiments, hMSCs (passage <6) were seeded at a density of 10000 viable cells/cm^2, as determined by exclusion of Trypan blue, and cultured for 3–4 days prior to end point experiments.

Inhibitor Study

hMSCs were exposed to various inhibitor concentrations for 48 h to determine optimal concentrations. The following inhibitors and concentrations were used: 30 μM BTT 3033 (Integrin $\alpha_2\beta_1$ inhibitor, Tocris, Avonmouth, Bristol, U.K.), 30 μM P11 (Integrin $\alpha_v\beta_3/\alpha_v\beta_5$ inhibitor, Tocris) and 1 mg/mL GAP26 (Connexin-43 peptide-based inhibitor). GAP26 (Val-Cys-Tyr-Asp-Lys-Ser-Phe-Pro-Ile-Ser-His-Val-Arg) peptide was synthesized by standard solid-phase fluorenylmethyloxycarbonyl chloride chemistry on a Rink amide-MBHA resin using PS3 synthesizer (Protein Technologies, Tucson, AZ). These peptides were cleaved and deprotected in trifluoroacetic acid/thioanisole/ethanedithiol/anisole (90/5/3/2). The formation of peptide was characterized by liquid chromatography–mass spectrometry (LC–MS) (Figure S10).

For the inhibition experiment, the indicated concentrations of inhibitors were added to hMSC suspensions before seeding the cells onto the substrates. Cells were cultured for 4 days before harvesting RNA for gene expression analysis.

Measuring Levels of Intracellular Reactive Oxygen Species (ROS)

hMSCs were incubated with 10 μM 5-(and-6)-chloromethyl-2′,7′-dichlorodihydrofluorescein diacetate acetyl ester (DCFDA) (Life Technologies) in serum-free DMEM for 30 min following the manufacturer’s instructions. Cells were trypsinized and run on a FACS Calibur flow cytometer (BD Biosciences, Franklin Lakes, NJ) with the appropriate unstained control. $N = 3$ biological replicates were conducted per substrate condition. Data were analyzed by FlowJo software (Tree Star Inc., Ashland, OR).

Super Resolution Imaging

hMSCs were fixed with 4% paraformaldehyde (PFA, Sigma-Aldrich) for 15 min at room temperature, washed three times with 1× PBS, and then permeabilized with 0.3% Triton X-100 (Sigma-Aldrich) for 5 min at room temperature. Primary anti-paxillin (catalog no. 610051, BD Transduction Laboratories, Franklin Lakes, NJ) and secondary AlexaFluor 568 goat anti-mouse (catalog no. A11004, Life Technologies) antibodies were diluted in 10% bovine serum albumin (Sigma-Aldrich) at 1:200 and 1:100, respectively, and centrifuged at 13000 rpm for 10 min before use. Samples were blocked in 10% bovine serum albumin for 20 min at room temperature, and primary antibody incubation occurred at room temperature for 1 h and 45 min, washed three times with 1× PBS, and then secondary antibody incubation for 1 h at room temperature followed by three washes with 1× PBS. Cells were mounted in Vectashield (H-1000, Vector Laboratories, Inc. Burlingame, CA) mounting medium. Structured illumination microscopy (SIM) imaging was performed on a GE Healthcare DeltaVision OMX equipped with a 60× 1.42 NA Oil objective and sCMOS camera. Images were collected from $N = 3$ biological replicates with $n \geq 3$ images per replicate. SIM images with a maximum projection (in Z) of 3D acquisitions were analyzed using ImageJ (National Institutes of Health, Bethesda, MD). Focal adhesion width was calculated using the ImageJ 1D line tool (width = 10) by drawing a line across the leading edge of the cell. A 1D plot of pixel intensity was generated live as the line was drawn to identify the focal adhesion regions within the plot. Full width at half-maximum (fwhm) was used as the width measurement for each focal adhesion. The average from at least 40 cells from three images was reported for each group.

Western Blot

Western blot analysis was done according to standard protocols.[26] Primary antibodies used in this study include: Integrin-α2 (1:200, sc-6586r, Santa Cruz Biotechnology, Dallas, TX), Integrin-β3 (1:200, D7X3P, Cell Signaling Technologies, Danvers, MA), Integrin-β5 (1:200, D24A5, Cell Signaling Technologies), Connexin-43 (1:200, #3512, Cell Signaling Technologies), and GAPDH (1:5000, 14C10, Cell Signaling Technologies). Appropriate secondary antibodies from Li-COR (Lincoln, NB) were used to image the blots on the Odyssey imaging system according to the manufacturer's protocol.

Immunocytochemistry and Immunophenotyping by Flow Cytometry

hMSCs were fixed with 4% paraformaldehyde (PFA, Sigma-Aldrich) for 15 min, permeabilized with 0.3% Triton-X (Sigma-Aldrich) for 15 min when probing intracellular targets, and blocked with 10% goat serum (Sigma-Aldrich) for >2 h, all at room temperature. hMSCs were then incubated with primary antibody in 1% bovine serum albumin (Supplementary Table S2) overnight at 4 °C, followed by incubation with the appropriate secondary antibody at 1:500 in 5% goat serum for 2 h at room temperature, and counterstained with Hoechst (2 μg/mL, Sigma-Aldrich). For staining the actin cytoskeleton, cells were incubated with Alexa488-phallodin (1:40 v/v in PBS, Life Technologies) for 10 min followed by counterstaining with Hoechst (2 μg/mL, Sigma-Aldrich) for 20 min at room temperature. Imaging was performed with either a Nikon Ti inverted microscope (Nikon Instruments Inc., Melville, NY, USA) or a Zeiss LSM 710 confocal microscope (Carl Zeiss, Oberkochen, Germany), and images were processed with ImageJ (National Institutes of Health).

For flow cytometry, unstained hMSCs were used to set voltages for the fluorescence and scatter channels. Single-stained hMSCs were used to determine compensation values so that fluorescence signal within one channel was definitively from a positively stained cell. Cells were then run on a FACS Calibur flow cytometer (BD Biosciences). Each experiment represents 10000 gated cells, and data were analyzed by FlowJo software (Tree Star Inc., Ashland, OR).

Quantitative Real-Time Polymerase Chain Reaction (cPCR and qRT-PCR)

hMSCs on spin-coated substrates were homogenized with the Trizol reagent (Life Technologies), mixed with chloroform (1:5 Trizol:chloroform), and separated by centrifugation (12000*g*, 15 min, 4 °C). The RNA contained within the aqueous phase was then isolated with RNeasy columns (Bio-Rad, Hercules, CA), according to the manufacturer's instructions. cDNA was synthesized using a kit (Applied Biosystems, Life Technologies), and qRT-PCR was performed with a SYBR Green master mix (Bio-Rad) with 15–20 ng cDNA and 500 nM each of forward and reverse primers, using a CFX Real-

Time PCR System (Bio-Rad). The qRT-PCR protocol included: 95 °C for 3 min, followed by 40 cycles of denaturation at 95 °C for 30 s, annealing at 58 °C 30 s, and extension at 72 °C for 30 s. The expression of each gene of interest was normalized to expression of glyceraldehyde 3-phosphate dehydrogenase (GAPDH) as a housekeeping gene, generating the $\Delta C(t)$ value. In Figure 1, the $\Delta C(t)$ values for *NANOG* or *SOX2* are scaled ($\times 10^5$) and reported because the experiment was repeated 5 times with 1 biological replicate per experiment, making normalization to TCPS errorless and therefore inaccurate. However, in remaining figures, the $2^{-\Delta\Delta C(t)}$ expression relative to the TCPS control is reported, in which $n \geq 3$ biological replicates for each experiment was reported. Primer sequences are listed in Supplementary Table S1, and only those that showed single, specific amplicons were used for qRT-PCR experiments.

Measuring Cell Proliferation

hMSCs were incubated with 10 μM 5-ethynyl-2′-deoxyuridine (EDU) (Life Technologies, Carlsbad, CA) in serum-free media for 12 h before completion of the 96-h culture period. Cells were fixed in 4% paraformaldehyde (PFA, Sigma-Aldrich, St. Louis, MO) and processed per the manufacturer's instructions. Images were taken with a Zeiss LSM 710 microscope (Carl Zeiss, Oberkochen, Germany), and the images were processed with Zeiss Zen software and ImageJ (National Institutes of Health, Bethesda, MD). $N = 6$ biological replicates were used per substrate condition.

Statistical Analysis

Comparisons between two groups were performed with a Student's unpaired t test. Comparisons between multiple groups were performed with a one- or two-way analysis of variance (ANOVA) with a Tukey post hoc test to adjust p-values for multiple comparisons. In all cases, $p < 0.05$ is considered statistically significant. Mean ± standard deviation is reported, unless otherwise noted.

RESULTS

Synthesis of a Three-Component Copolymer Library and Characterization of hMSC Pro-stemness, Low-Redox Phenotype

We first employed 2D copolymer substrates consisting of three subunits (Figure 1A): PCL, which is hydrophobic and protein adsorptive; PEG (2 kDa chain length), which is hydrophilic and cell-repellant; and carboxylated-PCL (cPCL), which is hydrophilic but interacts favorably with proteins. We included cPCL as a material "rescue" against the repellant effect of PEG, comparing two materials with the same mol % PEG, but with and without cPCL, allowing us to better understand how PEG repellency modulates stem cell behavior. Protein adsorption (Figure 1B) and contact angle (Figure 1C) were controlled by altering the mol % PEG, with increasing PEG content resulting in more hydrophilic, protein-repellant surfaces; this effect was counteracted upon inclusion of cPCL. The Young's modulus (near-surface modulus) of each surface was measured with atomic force microscopy, which revealed that moduli were constrained between 4 and 18 kPa (Figure S1). Typically, materials less than 1 kPa are required to disrupt the mechanotransduction response,[8] so the material elasticity was not expected to play a significant role in modulating cell behavior in this system. hMSCs formed aggregates on PEG–PCL copolymers but spread on 100%PCL and cPCL-containing materials (Figure 1D), verifying the functional repellency of PEG and adhesiveness of PCL and cPCL. These aggregates were three-dimensional in nature, formed directly following attachment (aggregates were observed as soon as 12 h postseeding), and comprised of a matrix-interactive layer upon which other cells adhered in preference of the cell-repellant surface.

We next evaluated copolymer-mediated modulation of *NANOG* and *SOX2*, two fundamental stemness genes that maintain self-renewal and differentiation capacity.[27,28] Con-firming our hypothesis that repellency would modulate stemness, one copolymer—10%PEG–90%PCL–induced a significant increase in expression of *NANOG* and *SOX2* relative to TCPS control (Figure 1E,F), with a concomitant reduction in intracellular ROS (Figure 1G and Figure S2). Furthermore, expression of STRO-1, the most commonly used in vivo marker of undifferentiated hMSCs, is gradually lost during in vitro culture on TCPS[29] but was reinstated on 10%PEG–90%PCL (Figure 1H). Increasing the mol % PEG further to 25% PEG–75% PCL resulted in large regions devoid of cell attachment due to a highly repellant surface (data not shown), which explains the decreased expression of stemness genes and indicates 25% PEG as the upper limit of cell repellency for further experiments.

Verification of Copolymer Film Surface Chemistry as the Primary Effector for hMSC Response

Copolymer surfaces were then precoated with adhesive fibronectin (FN) at varying concentrations to mask the repellent domains without changing copolymer composition. FN encouraged cell attachment and spreading while reducing aggregation (Figure 2A and Figure S3). After 8 h, hMSCs on uncoated and 0.05 $\mu g/cm^2$ FN-coated 10%PEG–90%PCL formed independent aggregates (red arrows), and after 72 h (Figure S4) cells had elongated but still favored cell–cell interactions as evidenced by aggregation. For qPCR, TCPS and substrate-free HDs were used as “no repellency” and “total repellency” controls, respectively. hMSCs on 10%PEG–90%PCL exhibited expression of *NANOG* and *SOX2* at levels similar to HDs, but this effect was reduced as FN concentration increased (Figure 2B,C). Of note, in most published biomaterial systems that aim to evaluate the role of stiffness, the material is coated with an adhesive protein layer that does not impede the material-derived effects; therefore, FN precoating also suggests that substrate stiffness is a less dominant effect than surface repellency in our system, since the stiffness of the underlying material is unchanged yet the observed stemness modulation is lost.

Investigation of Tuning hMSC Phenotype by Altering PEG Chain Size and Mole Percent

The length and/or mol % of the PEG subunit within the copolymer backbone was tuned to further regulate the cellular response. Copolymers containing (i) 5–20 mol % PEG and (ii) block lengths of 750 Da, 2 kDa, or 5 kDa (to be indicated by a subscript number) were synthesized and characterized (Figure S5). After 4 days in culture, PEG_{750} copolymers allowed attachment, although to a decreasing degree as mol % PEG increased (Figure 3A). This trend was more apparent on PEG_{2k} copolymers as >10 mol % PEG inhibited attachment, and virtually no attachment was observed on PEG_{5k} copolymers. Four materials (5%PEG_{750}, 20%PEG_{750}, 5%PEG_{2k}, and 10%PEG_{2k}) were chosen for remaining studies to represent two decoupled variables: (1) increased PEG chain size at a constant mol % and (2) increased mol % with constant PEG chain size (Figure 3A,B, red letters).

hMSCs on PEG_{750} copolymers interacted with the surface and elongated, but cells on PEG_{2k} copolymers generated more isolated aggregates (Figure 3B). The expression of *NANOG* (Figure 3C) and *SOX2* (Figure 3D) were heavily influenced by both the PEG chain length and the mol %. *NANOG* expression was increased significantly on all copolymers, relative to TCPS control, with a subsequent increase on 10%PEG_{2k}. Copolymers comprised of longer PEG chains (2 kDa versus 750 Da) stimulated greater expression of *SOX2* genes, and the increased mol % of PEG within each group (10/20% versus 5%) further enhanced this effect. On all copolymers, the expression of key antioxidative mediators, including sestrin 1 (*SESN1*), thioredoxin (*TRX*), superoxide dismutase 2 (*SOD2*), and apurinic endonuclease/redox-factor 1 (*APE/Ref-1*), was increased (Figure 3E,H), and intracellular ROS load (Figure 3I) was significantly reduced relative to TCPS.

Nano- and Angstrom-level Investigation of PEG and PCL Phase Separation

To understand how the polymer structure at the cell-material interface influences cell function, nanoscale features of the copolymer surfaces were examined by X-ray scattering (XRS). The small-angle XRS lamellar peak (Figure 4A) and the wide-angle XRS crystalline peaks (Figure 4B) associated with PCL domains were present in all samples, confirming that PEG does not interfere with the formation of PCL lamellae. Absence of PEG crystalline peaks in all samples—especially in PEG_{2k} and PEG_{5k} where PEG would be expected to crystallize—suggests that PEG crystallization is interrupted in the copolymers. Together, these two observations led us to conclude that PEG chains are embedded as amorphous segments within the amorphous domains of the semicrystalline PCL. However, the influence of PEG segments on the morphology of the copolymer depends on its chain length. For example, although the PCL crystallinity did not change in PEG_{750} copolymers upon hydration (Figure 4C), the medium-angle XRS became broad, indicating that the PCL chains in this copolymer become less ordered when wet (Figure S7). In contrast, the PCL crystallinity in 100%PCL, and in copolymers with PEG_{2k}, and PEG_{5k}, increased upon hydration, and the medium-angle XRS peak remained sharp, indicating that PCL crystalline order increased, or remains unchanged, upon hydration.

In most cases, crystallinity is known to decrease after wetting in crystalline polymers, especially polyelectrolytes, and water-soluble polymers such as poly(vinyl alcohol) (PVOH)[30] and PEG. But increases, or at least absence of any decrease that we observed in our polymers, have been reported in polymers such as poly(lactic acid) (PLA),[31] cellulose,[32] and polyamides.[33] In fact, a 5–10% increase in crystallinity in thick PCL scaffolds was reported upon exposure to water.[34] Thus, the reported crystallinity increases in submicron thick films over much shorter duration used in our experiments is not unexpected and can be attributed to the “plasticization” effect of water, where a small increase in the mobility of the polymer chains (PEG subunit) is able to “anneal” the polymer to a higher crystallinity (PCL subunit). With respect to our data, although PEG does not interfere with formation of PCL lamellae, its chain length-dependent distribution affects the characteristics of the lamellae (Figure 4D): shorter PEG segments in PEG_{750} copolymers are dispersed in the amorphous matrix and, therefore, decrease the PCL crystalline order when wet. In contrast, the longer PEG segments in PEG_{2k} and PEG_{5k} copolymers are excluded from amorphous PCL, and therefore allow for increased PCL crystallinity upon wetting. These excluded PEG segments form loops that swells upon hydration, mushrooming at the material surface and abrogating cell attachment (Figure 4E). Such loops account for the increase in the lamellar spacing upon hydration relative to 100%PCL in PEG_{2k} and PEG_{5k}, but not in PEG_{750} (PEG_{2k}/PEG_{5k}: 150–155 Å vs PCL: 140 Å vs PEG_{750}: 132 Å); that is, swelling PEG domains physically push the crystalline PCL lamellae apart when wetted (Figure 4D and Figure S8). Indeed, PEG loops engineered onto polymer surfaces have been leveraged to create antifouling surfaces,[35,36] explaining the enhanced cell-repellent effect of PEG_{2k} and PEG_{5k} copolymers. Therefore, the PEG chains exhibit a divergent, chain length-dependent effect in their modulation of hMSC behaviors. Embedded PEG_{750} chains are unable to collectively diffuse to the polymer–air/water interface, resulting in reduced repellency at a given mol %; PEG_{2k} and PEG_{5k} copolymers exert an enhanced repellency even at 5 mol % because, when hydrated, the phase-separated PEG chains form loops at the material surface that swell and mask the adhesive, noncrystalline PCL, augmenting the effect at each mol %.

To prove that hMSCs perceive the cell-material interface differently based upon PEG chain length, we visualized focal adhesion (FA) formation at the cell-material interface using super-resolution, structured illumination microscopy.[37] A key FA protein, paxillin, was chosen to represent nontransient adhesion complexes at the material surface (Figure 5). Cells cultured on glass and 100%PCL substrates had large FA sites, and both 5%PEG_{750} and 20%PEG_{750} copolymers allowed for FAs that displayed a similar morphology, confirming that shorter PEG chains do not interfere with cell binding at the material surface (Figure 5A). In contrast, 5%PEG_{2k} and 10% PEG_{2k} exhibited reduced FA width and sparser morphology. Decreasing FA width and extending long axes have been documented to correlate with weak cell-matrix binding,[38] and frustrated FAs observed on PEG_{2k} copolymers suggest weak cell-material interactions. When quantified, FA width was not different on PEG_{750} copolymers, relative to glass and 100%PCL, but significantly decreased on PEG_{2k} materials (Figure 5B). It is important to note that surface crystallinity of the substrates could affect the surface roughness, and thereby influence FA formation. However, on the basis of the data presented in Figure 4C, any differences in surface roughness caused by crystallinity are minimal as the wetted surfaces for all the copolymers had the same degree of crystallinity. Therefore, differences in FA morphology were responsive to the copolymer backbone chemistry (PEG steric hindrance effect).

Demonstration of Universal Copolymer Effect on Multiple, Aged hMSC Donors and Critical Role of CX43 in Pro-Stemness, Low-Redox Phenotype Adoption

To demonstrate that the effect of the material was not donor dependent, hMSCs from three patient sources were tested on the 5%PEG_{2k} copolymer since a strong cellular response was consistently observed on this substrate. For all donors, compared to TCPS, the expression of *NANOG* and *SOX2* was significantly increased on 5%PEG_{2k} (Figure 6A–C) and the expression of antioxidative genes was enhanced in virtually all cases (Figure 6D–F). Intracellular ROS levels decreased for all patient cells cultured on the copolymer, compared to TCPS control (Figure 6G). Since the balance of cell–cell and cell-matrix adhesions was hypothesized to drive this effect, we measured gene expression of multiple cell adhesion molecules and integrin subtypes (Figure 7A) and identified CX43, integrin $\alpha2$ (ITGA2), and integrins $\beta3/\beta5$ (ITGB3/B5) as candidate regulators of the material-derived effect. Protein-level expression increases were confirmed by Western blot (Figure 7B). Upon inhibition, we found that interruption of CX43 most potently attenuated the expression of stemness (Figure 7C) and antioxidative genes (Figure 7D). CX43 has recently been shown to maintain skin-derived stem cells,[39] and is also required for resistance to oxidative stress in the bone marrow;[40] this finding indicates a functional role of CX43 in mediating material-derived signals in hMSCs.

DISCUSSION

The data presented here are, to our knowledge, the first example of intrinsic copolymer properties regulating high-level functions of primary human stem cells. To date, most material systems have relied upon premeditated preparation of physicochemical substrate-derived cues to influence cell function, such as changing the cross-linking ratio of a hydrogel to alter stiffness, printing adhesive areas to control cell spreading, or directly imparting micro- and nanotopographical cues to the material surface. In contrast, the PEG–PCL copolymers used here entropically form phase-separated domains that ultimately impact cell function through alterations to the cell-material interface. This type of hands-off approach has been mostly unreported in the literature and is expected to generate useful insight and novel research questions for outside-in control of cell behavior. Furthermore, the specific ability to modulate the expression of classical stemness genes, as well as the intracellular redox capacity and associated antioxidative mechanisms, is especially novel in the biomaterials field, and linking how the material organization affects cell function is promising for ongoing work to design cell-instructive scaffolds.

The chemical composition of the copolymer heavily influenced protein adsorption, contact angle, and subsequent cell attachment (Figure 1). As we have reported previously,[19] the inclusion of the cPCL component reversed the cell-repellant effect of PEG, allowing for adequate cell attachment to the material surface despite up to 25 mol % PEG in the copolymer backbone. Indeed, protein adsorption to PEG-PCL-cPCL copolymers was significantly higher than the PEG-PCL counterparts, and similar to 100%PCL (Figure 1B). Increased expression of *NANOG* and *SOX2* on 10%PEG–90%PCL copolymers supported our hypothesis that cell-repellant materials would stimulate a beneficial, pro-stemness phenotype; however, the reduction in gene-level expression on 25%PEG–75%PCL copolymers was at first unexpected, but can be explained by an overabundance of PEG domains at the material surface. This results in a nonadhesive interface to which the cells cannot attach, and therefore represents an upper limit to the mol % PEG in the copolymer backbone that can be used as a culture substrate. For all copolymers ≤20 mol % PEG, cell aggregates maintained viability over the culture period, and could even be expanded and serially passaged for several weeks (data not shown). Cell health did not appear to be affected by the PEG chain length or mol %; however, copolymers composed of 750 Da PEG allow for substantial cell adhesion and spreading, but still stimulate a moderate increase in stemness gene expression. Therefore, 750 Da PEG chain length is considered to be the most optimal for long-term culture systems and future applications of semirepellant substrates for tissue engineering.

The concurrent reduction in intracellular ROS observed for cells cultured on PEG-PCL copolymers is suggestive of a more immature phenotype, since naïve stem cells are known to express high levels of stemness genes and maintain a low level of ROS.[41] The striking observation that these mesenchymal cells, which favor cell-matrix interactions over cell–cell adhesions, dynamically form aggregates at the material surface instead of simply detaching and undergoing apoptosis, as discussed earlier, suggests something intrinsic to the cell type that remains to be fully understood. The origin of the hMSC from the neural crest during development might provide initial insight: a highly cell–cell adhesive structure, yet one that undergoes immense locomotion and reorganization, the neural crest gives rise to the mesenchyme, and most of these cells are lost in the adult, but the MSC remains.[42] Therefore, it is possible that the highly cell–cell interactive aggregates activate a transcriptional and behavioral profile that is reminiscent of the developmental events. A report by Yu et al. demonstrated that miR-125b is an adhesion-dependent microRNA that protects hMSCs against anoikis in suspension culture.[43] Indeed, miR-125b plays various roles in cancer and tissue homeostasis,[44] and its cell-protective activity in suspended hMSCs is therefore unsurprising. A logical follow-up question from our study would investigate how miR-125b expression modulates the levels of *NANOG* and *SOX2* on repellant copolymers. An additional question to be raised in future research is to understand the exact types of adhesive ECM components that are being synthesized and secreted by hMSC aggregates, and to compare this profile against what is observed in the embryo. Furthermore, investigation into the dynamic turnover of ECM components in the extracellular space, and how they interact with repellant domains of the synthetic copolymers, will be highly interesting.

Finally, the XRS data of the copolymer library developed with careful chemical synthesis illustrated phase separation phenomena that had not previously been reported in the literature. The tight control of the volume fraction percent of PEG in the copolymers across each PEG chain length family (Figure S8) allowed for specific analysis of how the competing PEG and PCL chains were entropically interacting as PEG chain length and mol % were changed. While several copolymers synthesized for biomedical applications have distinct properties such as crystallinity, the semicrystalline nature PCL combined with varying PEG chain length provided ample variations in cell-adhesive and cell-repellent zones on the cell culture film surface. This natural assembly that can be regulated without postprocessing of the copolymer films, thereby minimizing potential fabrication complications or necessary reagents that could be cytotoxic. This strategy of copolymer assembly will hopefully inspire polymer chemists and biomedical researchers alike to revisit old polymer chemistries that compete with each other, with respect to a defined variable, and subsequently synthesize these copolymers to interrogate their naturally assembly in two-dimensional and three-dimensional structures.

CONCLUSION

These data indicate that the copolymers of moderate surface repellency regulate both hMSC stemness and redox potential and that this effect can be tuned by altering the nanoscale presentation of the repellent unit in the copolymer backbone. This is the first study to leverage intrinsic copolymer properties to regulate high-level stem cell function and demonstrates an intimate coupling of material surface chemistry and resultant changes to functional intracellular machinery. The findings from this interdisciplinary work advance our understanding of how material-derived cues rejuvenate adult stem cells in culture and will be used to develop cell-instructive scaffolds to enhance the translational capacity of hMSCs.

Supplementary Material

Refer to Web version on PubMed Central for supplementary material.

Acknowledgments

This research work was funded and supported by NSF CBET BME 1056046, NSF DMR BMAT 1506717, NIH EB 019509, and AHA GRNT25890018. D.A.B. was partially supported by the Vanderbilt Medical Scientist Training Program T32 Training Grant GM007347. This study was also supported in part by Vanderbilt CTSA Grant No. UL1 TR000445 from NCATS/NIH (VICTR Resource Request No. 12676). This study employed resources at the Vanderbilt Institute of Nanoscale Science and Engineering (VINSE), a facility renovated under NSF ARI-R2 DMR-0963361. Confocal microscopy was performed through the use of the VUMC Cell Imaging Shared Resource (supported by NIH Grant Nos. CA68485, DK20593, DK58404, HD15052, DK59637, and EY08126). ^{1}H NMR was conducted in the Small Molecule NMR Facility Core. Cornell CHESS (X-ray scattering experiments) is supported by the NSF & NIH/NIGMS via NSF Award No. DMR-1332208, and the MacCHESS resource is supported by NIGMS Award No. GM-103485. We thank Dr. Richard Gillilan for helping us with the synchrotron measurements. The authors acknowledge Pampee Young and Sue H. Lee for providing patient-derived MSCs and conducting technical works on biological assays, respectively.

References

1. Behfar A, Crespo-Diaz R, Terzic A, Gersh BJ. Cell therapy for cardiac repair–lessons from clinical trials. Nat Rev Cardiol. 2014; 11(4):232–46. [PubMed: 24594893]
2. Mendicino M, Bailey AM, Wonnacott K, Puri RK, Bauer SR. MSC-Based Product Characterization for Clinical Trials: An FDA Perspective. Cell Stem Cell. 2014; 14(2):141–5. [PubMed: 24506881]
3. Roobrouck VD, Ulloa-Montoya F, Verfaillie CM. Self-renewal and differentiation capacity of young and aged stem cells. Exp Cell Res. 2008; 314(9):1937–44. [PubMed: 18439579]
4. Stolzing A, Jones E, McGonagle D, Scutt A. Age-related changes in human bone marrow-derived mesenchymal stem cells: consequences for cell therapies. Mech Ageing Dev. 2008; 129(3):163–73. [PubMed: 18241911]
5. Wagner W, Bork S, Horn P, Krunic D, Walenda T, Diehlmann A, Benes V, Blake J, Huber FX, Eckstein V, Boukamp P, Ho AD. Aging and replicative senescence have related effects on human stem and progenitor cells. PLoS One. 2009; 4(6):e5846. [PubMed: 19513108]
6. Wagner W, Horn P, Castoldi M, Diehlmann A, Bork S, Saffrich R, Benes V, Blake J, Pfister S, Eckstein V, Ho AD. Replicative senescence of mesenchymal stem cells: a continuous and organized process. PLoS One. 2008; 3(5):e2213. [PubMed: 18493317]
7. Bara JJ, Richards RG, Alini M, Stoddart MJ. Concise review: Bone marrow-derived mesenchymal stem cells change phenotype following in vitro culture: implications for basic research and the clinic. Stem Cells. 2014; 32(7):1713–23. [PubMed: 24449458]
8. Engler AJ, Sen S, Sweeney HL, Discher D. EMatrix elasticity directs stem cell lineage specification. Cell. 2006; 126(4):677–89. [PubMed: 16923388]

9. Trappmann B, Gautrot JE, Connelly JT, Strange DG, Li Y, Oyen ML, Cohen Stuart MA, Boehm H, Li B, Vogel V, Spatz JP, Watt FM, Huck WT. Extracellular-matrix tethering regulates stem-cell fate. Nat Mater. 2012; 11(7):642–9. [PubMed: 22635042]
10. Wen JH, Vincent LG, Fuhrmann A, Choi YS, Hribar KC, Taylor-Weiner H, Chen S, Engler AJ. Interplay of matrix stiffness and protein tethering in stem cell differentiation. Nat Mater. 2014; 13:979. [PubMed: 25108614]
11. Dalby MJ, Gadegaard N, Tare R, Andar A, Riehle MO, Herzyk P, Wilkinson CD, Oreffo RO. The control of human mesenchymal cell differentiation using nanoscale symmetry and disorder. Nat Mater. 2007; 6(12):997–1003. [PubMed: 17891143]
12. Bartosh TJ, Ylostalo JH, Mohammadipoor A, Bazhanov N, Coble K, Claypool K, Lee RH, Choi H, Prockop DJ. Aggregation of human mesenchymal stromal cells (MSCs) into 3D spheroids enhances their anti-inflammatory properties. Proc Natl Acad Sci U S A. 2010; 107(31):13724–9. DOI: 10.1073/pnas.1008117107 [PubMed: 20643923]
13. Cheng NC, Chen SY, Li JR, Young TH. Short-term spheroid formation enhances the regenerative capacity of adiposederived stem cells by promoting stemness, angiogenesis, and chemotaxis. Stem Cells Transl Med. 2013; 2(8):584–94. [PubMed: 23847001]
14. Yao X, Peng R, Ding J. Cell-material interactions revealed via material techniques of surface patterning. Adv Mater (Weinheim, Ger). 2013; 25(37):5257–86.
15. Bernard AB, Lin CC, Anseth KS. A microwell cell culture platform for the aggregation of pancreatic beta-cells. Tissue Eng Part C. 2012; 18(8):583–92.
16. Hsu SH, Huang G. SSubstrate-dependent Wnt signaling in MSC differentiation within biomaterial-derived 3D spheroids. Biomaterials. 2013; 34(20):4725–38. [PubMed: 23562051]
17. Huang GS, Dai LG, Yen BL, Hsu S. HSpheroid formation of mesenchymal stem cells on chitosan and chitosan-hyaluronan membranes. Biomaterials. 2011; 32(29):6929–45. [PubMed: 21762982]
18. Sart S, Tsai AC, Li Y, Ma T. Three-Dimensional Aggregates of Mesenchymal Stem Cells: Cellular Mechanisms, Biological Properties, and Applications. Tissue Eng Part B. 2014; 20(5):365–380.
19. Crowder SW, Gupta MK, Hofmeister LH, Zachman AL, Sung HJ. Modular polymer design to regulate phenotype and oxidative response of human coronary artery cells for potential stent coating applications. Acta Biomater. 2012; 8(2):559–569. [PubMed: 22019760]
20. Weber N, Wendel HP, Kohn J. Formation of viscoelastic protein layers on polymeric surfaces relevant to platelet adhesion. J Biomed Mater Res Part A. 2005; 72(4):420–7.
21. Sader JE, Chon JWM, Mulvaney P. Calibration of rectangular atomic force microscope cantilevers. Rev Sci Instrum. 1999; 70(10):3967–3969.
22. Poon B, Rittel D, Ravichandran G. An analysis of nanoindentation in linearly elastic solids. Int J Solids Struct. 2008; 45(24):6018–6033.
23. Choi C, Chae S, Kim T, Jang M, Cho C, Nah J. Preparation and Characterizations of Poly(ethylene glycol)-Poly(ε-caprolactone) Block Copolymer Nanoparticles. Bull Korean Chem Soc. 2005; 26(4):523–528.
24. Stevens D, Watson H, LeBlanc M, Wang R, Chou J, Bauer W, Harth E. Practical polymerization of functionalized lactones and carbonates with Sn(OTf)2 in metal catalysed ringopening polymerization methods. Polym Chem. 2013; 4:2470–2474.
25. Deskins DL, Bastakoty D, Saraswati S, Shinar A, Holt GE, Young PP. Human mesenchymal stromal cells: identifying assays to predict potency for therapeutic selection. Stem Cells Transl Med. 2013; 2(2):151–8. [PubMed: 23362238]
26. Sung HJ, Yee A, Eskin SG, McIntire LV. Cyclic strain and motion control produce opposite oxidative responses in two human endothelial cell types. Am J Physiol: Cell Physiol. 2007; 293(1):C87–94. [PubMed: 17314265]
27. Go MJ, Takenaka C, Ohgushi H. Forced expression of Sox2 or Nanog in human bone marrow derived mesenchymal stem cells maintains their expansion and differentiation capabilities. Exp Cell Res. 2008; 314(5):1147–54. [PubMed: 18187129]
28. Tsai CC, Su PF, Huang YF, Yew TL, Hung SC. Oct4 and Nanog directly regulate Dnmt1 to maintain self-renewal and undifferentiated state in mesenchymal stem cells. Mol Cell. 2012; 47(2):169–82. [PubMed: 22795133]

29. Kolf CM, Cho E, Tuan RS. Mesenchymal stromal cells. Biology of adult mesenchymal stem cells: regulation of niche, self-renewal and differentiation. Arthritis Res Ther. 2007; 9(1):204. [PubMed: 17316462]

30. Hodge RM, Bastow TJ, Edward GH, Simon GP, Hill A. JFree volume and the mechanism of plasticization in water-swollen poly(vinyl alcohol). Macromolecules. 1996; 29(25):8137–8143.

31. Vyavahare, OV. Ph D Thesis. University of Massachusetts - Amherst, University of Massachusetts; Amherst, MA: 2015. Investigation of Hydration-induced Structural Rearrangements of Poly(lactic acid).

32. Park S, Johnson DK, Ishizawa CI, Parilla PA, Davis M. FMeasuring the crystallinity index of cellulose by solid state C-13 nuclear magnetic resonance. Cellulose. 2009; 16(4):641–647.

33. Murthy NS, Stamm M, Sibilia JP, Krimm S. Structural-Changes Accompanying Hydration in Nylon-6. Macromolecules. 1989; 22(3):1261–1267.

34. Lam CXF, Hutmacher DW, Schantz JT, Woodruff MA, Teoh SH. Evaluation of polycaprolactone scaffold degradation for 6 months in vitro and in vivo. J Biomed Mater Res Part A. 2009; 90a(3): 906–919.

35. Du H, Chandaroy P, Hui SW. Grafted poly-(ethylene glycol) on lipid surfaces inhibits protein adsorption and cell adhesion. Biochim Biophys Acta, Biomembr. 1997; 1326(2):236–248.

36. Kang T, Banquy X, Heo J, Lim C, Lynd NA, Lundberg P, Oh DX, Lee HK, Hong YK, Hwang DS, Waite JH, Israelachvili JN, Hawker CJ. Mussel-Inspired Anchoring of Polymer Loops That Provide Superior Surface Lubrication and Antifouling Properties. ACS Nano. 2016; 10(1):930–7. [PubMed: 26695175]

37. Gustafsson MG. Nonlinear structured-illumination microscopy: wide-field fluorescence imaging with theoretically unlimited resolution. Proc Natl Acad Sci U S A. 2005; 102(37):13081–6. [PubMed: 16141335]

38. Gardel ML, Schneider IC, Aratyn-Schaus Y, Waterman CM. Mechanical integration of actin and adhesion dynamics in cell migration. Annu Rev Cell Dev Biol. 2010; 26:315–33. [PubMed: 19575647]

39. Dyce PW, Li D, Barr KJ, Kidder GM. Connexin43 is required for the maintenance of multipotency in skin-derived stem cells. Stem Cells Dev. 2014; 23(14):1636–46. [PubMed: 24694074]

40. Taniguchi Ishikawa E, Gonzalez-Nieto D, Ghiaur G, Dunn SK, Ficker AM, Murali B, Madhu M, Gutstein DE, Fishman GI, Barrio LC, Cancelas JA. Connexin-43 prevents hematopoietic stem cell senescence through transfer of reactive oxygen species to bone marrow stromal cells. Proc Natl Acad Sci U S A. 2012; 109(23):9071–6. [PubMed: 22611193]

41. Wang K, Zhang T, Dong Q, Nice EC, Huang C, Wei Y. Redox homeostasis: the linchpin in stem cell self-renewal and differentiation. Cell Death Dis. 2013; 4:e537. [PubMed: 23492768]

42. Hay ED. The mesenchymal cell, its role in the embryo, and the remarkable signaling mechanisms that create it. Dev Dyn. 2005; 233(3):706–20. [PubMed: 15937929]

43. Yu X, Cohen DM, Chen C. SmiR-125b Is an Adhesion-Regulated microRNA that Protects Mesenchymal Stem Cells from Anoikis. Stem Cells. 2012; 30(5):956–964. [PubMed: 22331826]

44. Sun YM, Lin KY, Chen YQ. Diverse functions of miR-125 family in different cell contexts. J Hematol Oncol. 2013; 6:6. [PubMed: 23321005]

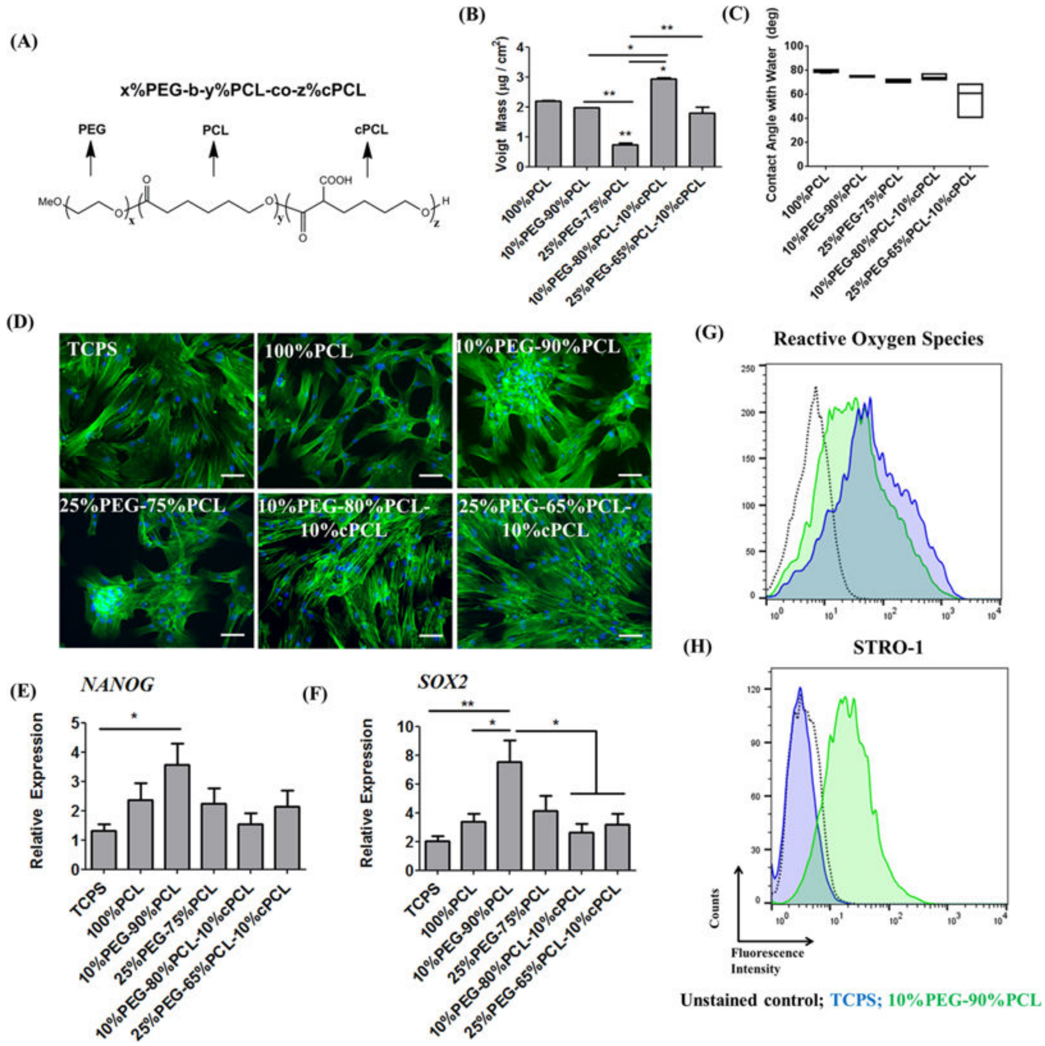

Figure 1.

Cell-repellency promotes stemness and reduces intracellular ROS. (A) Schematic representation of the copolymer structure, including hydrophobic and cell-adhesive PCL, hydrophilic and cell-repellent PEG, and hydrophilic and cell-adhesive cPCL. By varying the molar percentage of each subunit, (B) protein adsorption and (C) contact angle on spin-coated surfaces was controlled. Increasing PEG content resulted in a more repellent surface, but inclusion of the cPCL component increased protein binding. (D) Cell attachment and spreading were heavily influenced by the substrate upon which they were grown. hMSCs on TCPS or 100% PCL attached and spread normally, but copolymers of PEG–PCL forced cells to aggregate, discouraging cell-matrix interactions; in contrast, hMSCs cultured on the PEG–PCL-cPCL copolymers appeared similar to those on TCPS and 100% PCL, demonstrating that the cell-repellent PEG subunit has a functional effect on cell behavior (green, phalloidin; blue, Hoechst; scale bars = 100 *µ*m). The gene expression of the core stemness genes (E) *NANOG* and (F) *SOX2* was modulated by culture on the test substrates (*n* = 5). Furthermore, the accumulation of intracellular ROS (G) was decreased on 10% PEG–90% PCL, relative to TCPS, as indicated by the fluorescence of the ROS-sensitive

DCFDA dye. (H) The expression of STRO-1, an in vivo marker of undifferentiated hMSCs in the bone marrow, was lost during culture on TCPS but was reinstated following three-day culture on 10% PEG–90% PCL. All bars are mean ± SD $*p < 0.05$, $**p < 0.01$ as indicated between the lines.

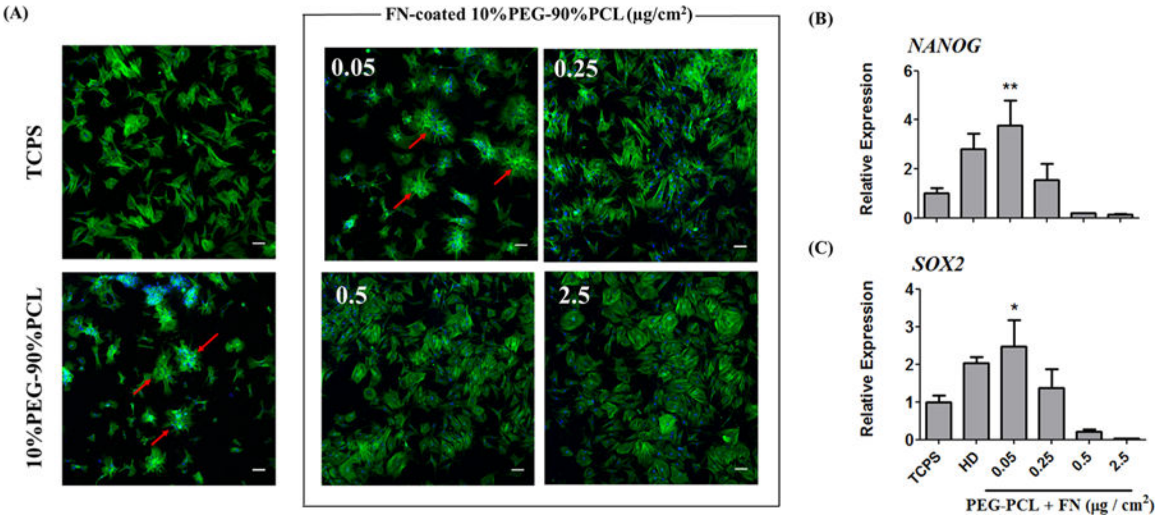

Figure 2.

Precoating copolymer surface with extracellular matrix protein abbrogates pro-stemness gene expression. (A) To prove that surface repellency is required to modulate stemness, 10%PEG–90%PCL was precoated with fibronectin (FN) at various concentrations before culture (green, phalloidin; blue, Hoechst; scale bars = 100 μm). On uncoated and 0.05 μg/cm^2 FN 10%PEG–90%PCL, hMSCs formed aggregates (red arrows) at 8 h postseeding. Increasing FN concentration enhanced cell attachment and spreading beyond what was observed on TCPS control. The expression of (B) *NANOG* and (C) *SOX2* was regulated by the surface repellency ($n = 4$). At the lowest FN concentration, 10%PEG–90%PCL copolymers promoted expression of stemness genes that was similar to that of substrate-free hanging drop (HD) cultures; however, as FN concentration increased, cell attachment and spreading increased, and the increased stemness effect was lost. All bars are mean ± SD $*p < 0.05$, $**p < 0.01$ relative to TCPS.

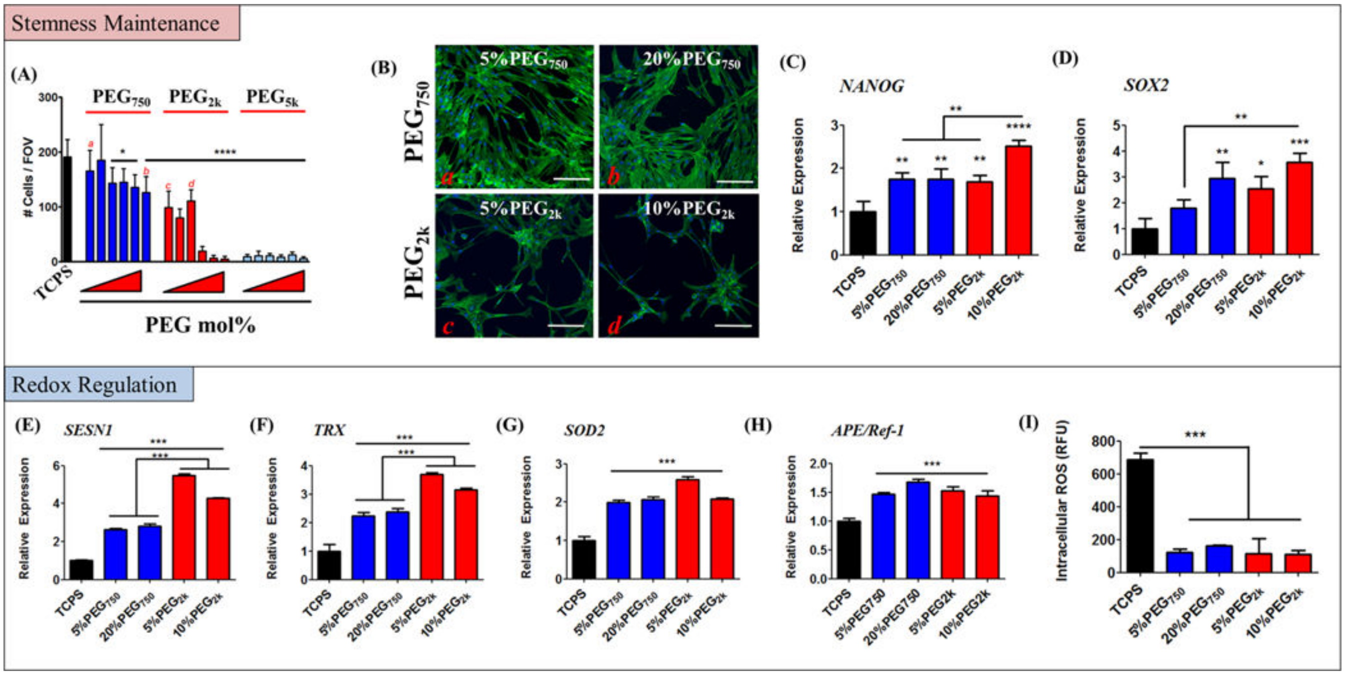

Figure 3.

Tuning PEG chain length and mol % regulates cell attachment, stemness gene expression, and redox potential. (A) Cell attachment could be tuned by varying the PEG mol % and/or chain length within the copolymer. All 750 Da PEG copolymers (PEG_{750}) and 2 kDa PEG (PEG_{2k}) ≤ 10 mol % maintained hMSC attachment, whereas PEG_{2k} copolymers >10 mol % and the entire 5 kDa PEG (PEG_{5k}) library prevented cell attachment. Therefore, four materials (indicated by the red letters) were chosen as they offered the greatest range of PEG mol % and/or PEG chain length without completely preventing cell attachment. (B) hMSCs cultured on PEG_{750} copolymers attached and elongated but still formed aggregates (*a*, 5%PEG_{750}, and *b*, 20%PEG_{750}). In contrast, at the same PEG mol % or less, PEG_{2k} copolymers discouraged cell attachment and promoted cell aggregation at the material surface (*c*, 5%PEG_{2k}, and *d*, 10%PEG_{2k}). (C, D) PEG mol % percentage and chain length both affected the gene expression of stemness markers significantly. The expression of *NANOG* was enhanced on all copolymers relative to TCPS, with greatest expression on 10%PEG_{2k}. *SOX2* was higher on 20%PEG_{750} versus 5%PEG_{750}, and the increase in PEG chain length enhanced this effect further, with 5%PEG_{2k} expression higher than 5%PEG_{750} and 10%PEG_{2k} higher than 20%PEG_{750} ($n = 3$). Furthermore, the expression of antioxidative genes was enhanced significantly in hMSCs cultured on all test polymers, compared to TCPS control (G, H). The expression of (E) *SESN1* and (F) *TRX* was further increased on PEG_{2k} copolymers ($n = 3$). (I) Enhanced redox gene expression was functionally relevant as hMSCs from all copolymers exhibited significantly reduced intracellular ROS. All bars are mean ± SD $*p < 0.05$, $**p < 0.01$, $***p < 0.001$, $****p < 0.0001$ relative to TCPS or as indicated between the lines.

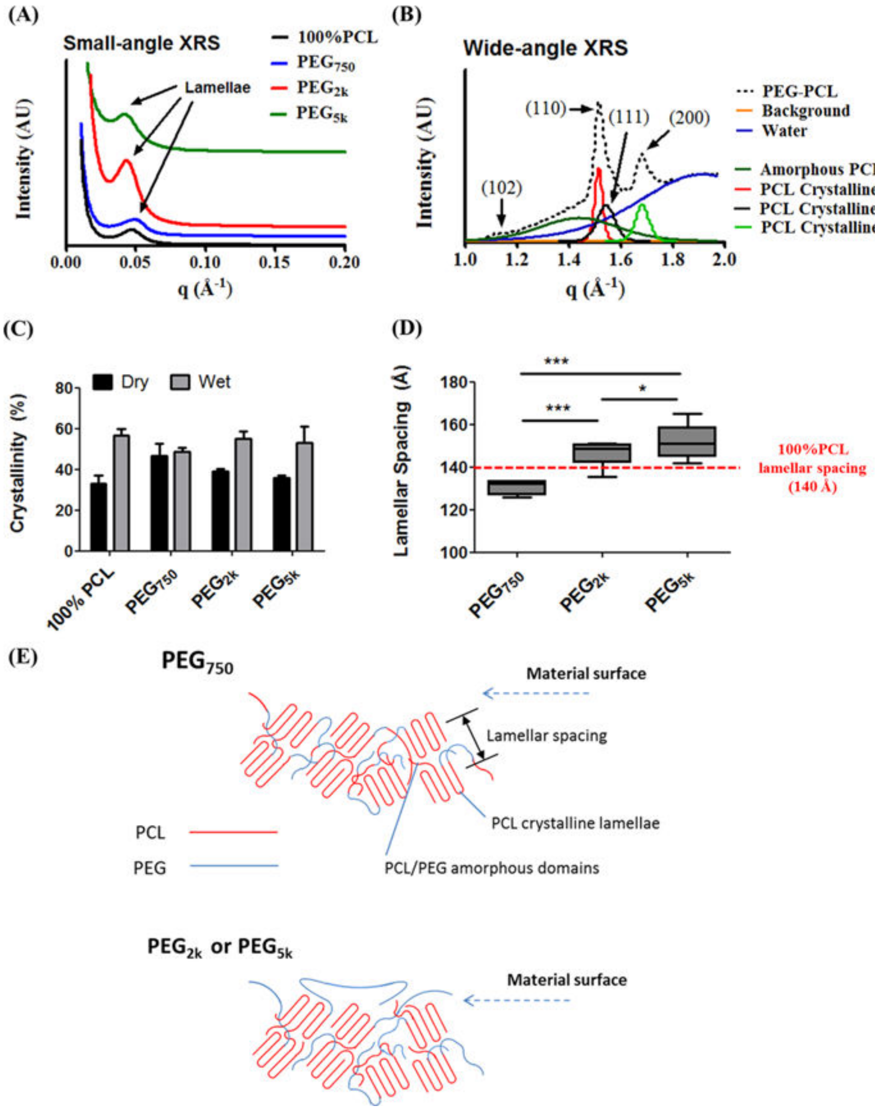

Figure 4.

X-ray scattering (XRS) reveals PEG chain length-dependent nano- and angstrom-scale characteristics at the material surface. (A) Small-angle and (B) wide-angle XRS confirmed the presence of PCL lamellae and crystalline structures, respectively, in all test copolymers (sample curves shown). Small-angle XRS data indicate that PEG chain length does not interfere with lamellar formation. Wide-angle XRS data demonstrate that the example curve of measured PEG–PCL spectra is the summation of signals from amorphous PCL, three peaks of crystalline PCL, and water. (C) PEG_{750}, but not PEG_{2k} or PEG_{5k}, prevented PCL crystallization under wet conditions, suggesting that PEG_{750} chains interdigitate within PCL domains whereas the longer PEG chains remain excluded but mushroom out at the polymer–air/water interface. (D) Indeed, lamellar spacing data further support this claim. PEG_{2k} and PEG_{5k} chains swelled upon hydration, physically distancing the adjacent crystalline domains of PCL. (E) Schematic representation of PEG chain length-dependent interactions with the PCL matrix. In PEG_{750} samples, PEG chains remain interdigitated in the amorphous PCL matrix and cannot mobilize to the material surface upon wetting. In contrast, larger PEG chains (PEG_{2k}, PEG_{5k}) are completely excluded from the PCL region, forming a loop that hydrates and swells, effectively mushrooming out and masking the adhesive PCL domains. All bars are mean ± SD *$p < 0.05$, and *** $p < 0.001$ between groups indicated by the lines.

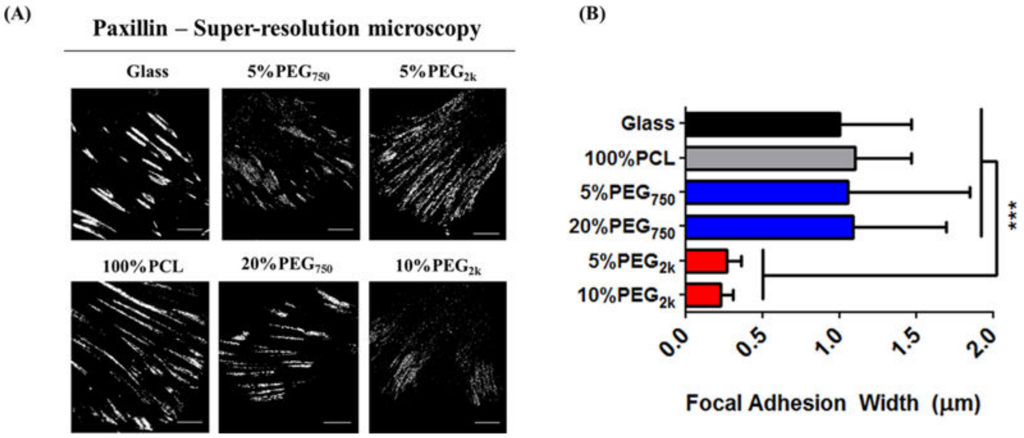

Figure 5.

Focal adhesion formation is disrupted by PEG_{2k}, but not PEG_{750}, chains. (A) To interrogate how cells perceive the nanoscale surface, super resolution, structured illumination microscopy (SIM) was performed for the mature focal adhesion (FA) protein, paxillin. On glass and 100% PCL surfaces (i.e., fully adhesive, nonrepellent), hMSCs formed thick, dense FAs. Similarly, on PEG_{750} copolymers, FA morphology and width remained similar to the adhesive controls; however, on PEG_{2k} samples, FAs were sparse with a compromised, thin morphology, suggesting weak cell-matrix interactions and supporting the presentation of PEG_{2k} chains at polymer–air/material interface (scale bars = 5 μm). (B) Quantification of FA width confirms similarity between glass, 100% PCL, and PEG_{750} samples versus PEG_{2k}. All bars are mean ± SD $*p < 0.05$, and $*** \ p < 0.001$ between groups indicated by the lines.

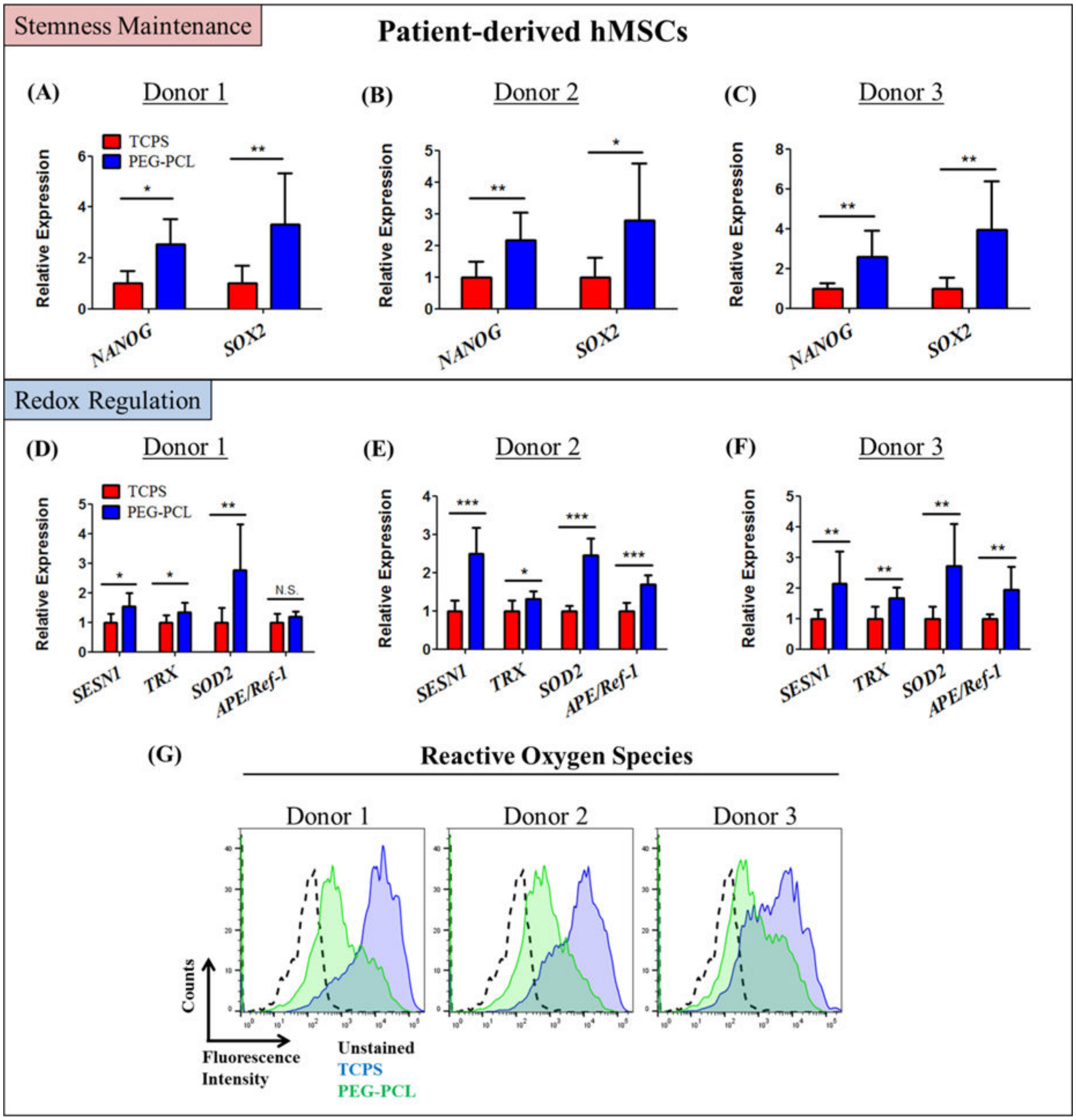

Figure 6.

Patient-derived hMSCs demonstrate that material-mediated modulation of stemness and redox is not donor-specific. (A–C) hMSCs isolated from three different donors demonstrated significant increases in the expression of *NANOG* and *SOX2* when cultured on 5%PEG$_{2k}$, relative to TCPS control ($n = 4$). (D–F) Similarly, the expression of the antioxidative genes *SESN1*, *TRX*, *SOD2*, and *APE/Ref-1* was downregulated in virtually all cases ($n \geq 5$). (G) Intracellular ROS load was also reduced for hMSCs isolated from all three donors when cultured on 5%PEG$_{2k}$, relative to the TCPS counterpart. All bars are mean ± SD $*p < 0.05$, $**p < 0.01$, $***p < 0.001$ relative to TCPS or as indicated between the lines.

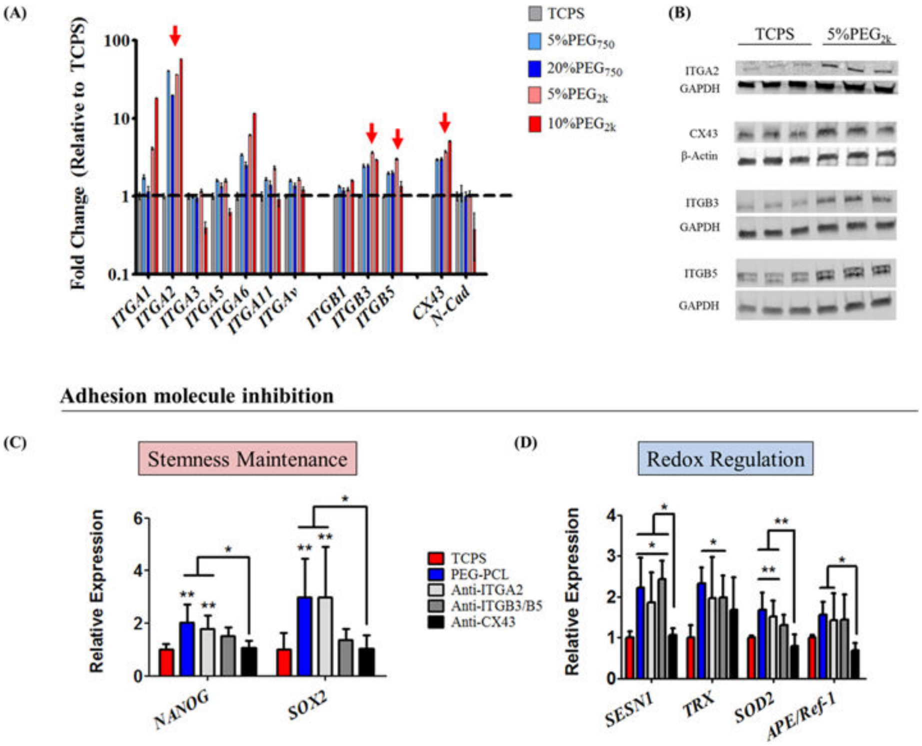

Figure 7.

Inhibition of adhesion proteins suggests a role for connexin-43 (CX43) in regulating the outside-in signaling. (A) In order to identify which cell–cell/cell–matrix adhesion molecule(s) played a role in modulating the signaling, gene expression profiling of several integrin subtypes and cell adhesion molecules was performed. The most promising candidates were those marked with red arrows, including *ITGA2*, *ITGB3*, *ITGB5*, and *CX43*. (B) Western blot analysis of the most signficiantly upregulated cell–cell and cell–matrix adhesion molcules confirmed that protein-level changes reflected those observed at the gene level. Therefore, these proteins were hypothesized to be responsible for hMSCs adopting the pro-stemness, low-redox phenotype. Specific inhibition using small molecules or peptides was performed against integrin α2 (ITGA2), integrins β3 and β5 (ITGB3/B5), and connexin-43 (CX43) for commercial hMSCs cultured on 5%PEG$_{2k}$. (C) The gene expression of stemness markers significantly decreased when treated with anti-CX43 inhibitor, relative to untreated cells on 5%PEG$_{2k}$. (D) Similarly, the polymer-mediated increase in expression of *SESN1*, *SOD2*, and *APE/Ref-1* antioxidative genes was lost upon treatment with anti-CX43 inhibitor ($n \geq 5$). All bars are mean ± SD $*p < 0.05$, $**p < 0.01$ relative to TCPS or as indicated between the lines.